

Shaping Energy Exchange with Gyroscopic Interconnections: a geometric approach

Jasper Juchem* and Mia Loccufier

Department of Electromechanical, Systems and Metal Engineering, Ghent University

Email: *jasper.juchem@UGent.be

Abstract—Gyroscopic interconnections enable redistribution of energy among degrees of freedom while preserving passivity and total energy, and they play a central role in controlled Lagrangian methods and IDA-PBC. Yet their quantitative effect on transient energy exchange and subsystem performance is not well characterised.

We study a conservative mechanical system with constant skew-symmetric velocity coupling. Its dynamics are integrable and evolve on invariant two-tori, whose projections onto subsystem phase planes provide a geometric description of energy exchange. When the ratio of normal-mode frequencies is rational, these projections become closed resonant Lissajous curves, enabling structured analysis of subsystem trajectories.

To quantify subsystem behaviour, we introduce the inscribed-radius metric: the radius of the largest origin-centred circle contained in a projected trajectory. This gives a lower bound on attainable subsystem energy and acts as an internal performance measure. We derive resonance conditions and develop an efficient method to compute or certify the inscribed radius without time-domain simulation.

Our results show that low-order resonances can strongly restrict energy depletion through phase-locking, whereas high-order resonances recover conservative bounds. These insights lead to an explicit interconnection-shaping design framework for both energy absorption and containment control strategies, while taking responsiveness into account.

Index Terms—Gyroscopic systems, closed Lissajous curves, resonance, port-Hamiltonian systems, passivity-based control, geometric control.

I. INTRODUCTION

Energy-based control provides structure-preserving tools to shape closed-loop dynamics by manipulating storage, exchange, and dissipation while retaining passivity. Two complementary paradigms, controlled Lagrangians (CL) and interconnection-and-damping assignment passivity-based control (IDA-PBC), systematically modify kinetic/potential energies and the interconnection structure to achieve stabilisation and performance objectives without destroying the underlying mechanics [1]–[6]. In both, gyroscopic interconnections, which are skew-symmetric velocity couplings, play a central role: they redistribute energy among degrees of freedom without injection or dissipation, preserve the Hamiltonian/port-Hamiltonian structure, and are compatible with dissipativity analysis [7]–[10]. Yet, despite their widespread use, there remains a lack of quantitative, design-ready metrics that predict how gyroscopic couplings shape transient energy exchange between subsystems and how resonance constrains attainable performance.

We address this gap for a conservative two-DOF system with a constant skew-symmetric velocity coupling. The dynamics are integrable and evolve on invariant two-tori, so subsystem energy exchange admits a geometric description via projection onto the subsystem phase planes. When the ratio of the modal frequencies is rational, the projection closes to a finite Lissajous curve, exposing the resonance structure of the interconnection and enabling exact geometric envelopes and sharp number-theoretic criteria. For near-irrational ratios the projection becomes dense, recovering conservative bounds [11], [12]. This observation interfaces naturally with interconnection shaping: since the coupling parameter n determines the modal frequency split, tuning n selects the resonance class and thereby the achievable exchange. Related ideas of *tunable coupling* and *mode interaction* appear in engineered resonators, where coupling is modulated to route energy between modes. Examples include dynamic electrostatic modulation in gyroscopic ring resonators, frequency-mismatch compensation and mode matching in dual-mass gyroscopes, and analyses that explicitly target energy transfer between drive and sense modes [13]–[16]. These strands motivate a control-oriented quantification of energy routing induced by gyroscopic interconnections.

Building on the projected-torus geometry, we introduce the *resonant inscribed radius*, defined as the radius of the largest origin-centered circle contained in the projected trajectory of a subsystem. This radius is a lower bound on the subsystem energy that always remains, thus quantifying the strongest achievable depletion via gyroscopic exchange. We derive exact resonance conditions and a sharp degeneracy criterion (vanishing radius) and, for the nondegenerate cases, present an efficient certification method with a uniform error bound. Because the metric depends on the coupling only through the induced frequency ratio, it becomes a tunable performance knob: choosing n selects a rational or near-irrational ratio and hence the attainable exchange-depth and time-to-exchange. From a control perspective, this yields two complementary design objectives—*absorption* (maximize transfer away from the host subsystem) and *containment* (guarantee a nonzero retained energy)—with responsiveness constraints that trade depth of exchange against beat-time. This perspective complements potential/damping shaping in CL/IDA-PBC by exploiting the geometric resonance features of gyroscopic interconnections while preserving passivity and port-Hamiltonian structure [3], [6], [8], [17]. Applications that benefit from targeted energy

routing include vibration mitigation and energy funneling toward single actuation points [18].

Contributions and organization. We (i) provide a geometric account of subsystem exchange via invariant-torus projections and closed Lissajous curves at resonant pairs; (ii) derive exact resonance conditions together with a number-theoretic degeneracy criterion for vanishing inscribed radius; (iii) develop an efficient computation/certification method with a uniform error bound, and (iv) translate these insights into an interconnection-shaping design that selects n for *absorption* or *containment* under responsiveness constraints. Section II introduces the model and resonant pairs. Section III develops the geometry of the projections, envelopes, the resonant inscribed radius, and the degeneracy criterion together with a certified computation method. Section IV formulates the design problems and their trade-offs. Section V presents examples, and Section VI concludes.

II. MODEL AND RESONANT PAIRS

Consider

$$\ddot{q} + n\dot{z} + q = 0, \quad \ddot{z} - n\dot{q} + z = 0, \quad (1)$$

with state $(q, \dot{q}, z, \dot{z}) \in \mathbb{R}^4$ and constant gyroscopic coupling $n \in \mathbb{R}$.

A. Canonical form and Hamiltonian

Define $x = (q, z)^\top$, $p = (\dot{q}, \dot{z})^\top$, and the skew matrix $J = \begin{bmatrix} 0 & n \\ -n & 0 \end{bmatrix}$. Then (1) is equivalent to

$$\dot{x} = p, \quad \dot{p} = -x - Jp. \quad (2)$$

Proposition 1 (Hamiltonian structure and energy conservation). *With the standard symplectic form, the Hamiltonian $H(x, p) = \frac{1}{2}(\|x\|^2 + \|p\|^2)$ yields the dynamics above. Moreover, $\dot{H} = p^\top \dot{p} + x^\top \dot{x} = -p^\top Jp = 0$ since $J^\top = -J$.*

This is the canonical gyroscopic setting [5], [19]. The Hamiltonian of a subsystem is given by

$$H_k(k, \dot{k}) = \frac{1}{2}(k^2 + \dot{k}^2) \quad (3)$$

with $k \in \{q, z\}$.

B. Resonant pairs

Introduce $u = q + iz$. Then (1) reduces to

$$\ddot{u} - in\dot{u} + u = 0. \quad (4)$$

The characteristic equation for $u \sim e^{\lambda t}$ is $\lambda^2 - in\lambda + 1 = 0$, with imaginary roots $\lambda = i\Omega_1$ and $\lambda = -i\Omega_2$ where we define the *positive* modal frequencies

$$\Omega_1 := \frac{\sqrt{n^2 + 4} + n}{2}, \quad \Omega_2 := \frac{\sqrt{n^2 + 4} - n}{2}, \quad \Omega_1\Omega_2 = 1. \quad (5)$$

Thus the general solution is

$$u(t) = C_1 e^{i\Omega_1 t} + C_2 e^{-i\Omega_2 t}, \quad (6)$$

a quasi-periodic flow on invariant two-tori in the full 4D phase space [11].

Definition 1 (Resonant pair). Let $\Omega_1, \Omega_2 > 0$ be the modal frequencies defined in (5). A pair $(\tau, \sigma) \in \mathbb{N}^2$ with $\gcd(\tau, \sigma) = 1$, also referred to as being *coprime*, is called a *resonant pair* if

$$\frac{\Omega_1}{\Omega_2} = \frac{\tau}{\sigma} \in \mathbb{Q}.$$

Without loss of generality, we assume that $\tau > \sigma$.

Proposition 2 (Resonance condition). *The projected motions on (q, \dot{q}) and (z, \dot{z}) are periodic (closed Lissajous curves) if and only if (Ω_1, Ω_2) is a resonant pair. In terms of n this is equivalent to*

$$n^2 = \frac{(\tau - \sigma)^2}{\tau\sigma}. \quad (7)$$

Proof. The ratio of basic frequencies is rational if and only if the 2-torus flow is periodic when projected to time [11, Proposition 1.5.1, p. 33]. Solving $\frac{\Omega_1}{\Omega_2} = \frac{\sqrt{n^2 + 4} + n}{\sqrt{n^2 + 4} - n} = \frac{\tau}{\sigma}$ for n yields (7). \square

We discern two classes of resonant pairs:

Definition 2 (Low-order resonance pair). A resonant pair (τ, σ) is called *low-order* if it belongs to a fixed finite set

$$\mathcal{R}_{\text{low}} = \{(\tau, \sigma) \in \mathbb{N}^2 : \gcd(\tau, \sigma) = 1, \tau + \sigma \leq M\},$$

for some $M \in \mathbb{N}$. Low-order resonance pairs correspond to strong phase locking between the modal components, a phenomenon represented by the characteristically wide Arnold tongues associated with small ratios [12, Section 3.2.4].

Definition 3 (High-order resonance pair). A sequence of resonant pairs $\{(\tau_k, \sigma_k)\}$ is called *high-order* if

$$\tau_k + \sigma_k \rightarrow \infty \quad \text{and} \quad \frac{\tau_k}{\sigma_k} \rightarrow 1, \quad \text{with} \quad (\tau_k, \sigma_k) \neq (\tau, \tau),$$

equivalently if

$$\tau_k, \sigma_k \rightarrow \infty \quad \text{and} \quad |n| = \frac{|\tau_k - \sigma_k|}{\sqrt{\tau_k \sigma_k}} \rightarrow 0.$$

Hence, high-order resonance pairs correspond to weak phase locking and asymptotically dense sampling of the invariant torus [12].

III. SUBSYSTEM PROJECTION: LISSAJOUS CURVES

For the impulse disturbance class

$$\mathcal{D} := \{(q, \dot{q}, z, \dot{z})(0) = (0, \dot{q}_0, 0, 0) : |\dot{q}_0| \leq D\}, \quad (8)$$

with $D \in \mathbb{R}_{>0}$, solving (6) for C_1, C_2 gives $C_2 = -C_1 = i\rho_0$ with

$$\rho_0 := \frac{\dot{q}_0}{\Omega_1 + \Omega_2} = \frac{\dot{q}_0}{\sqrt{n^2 + 4}}. \quad (9)$$

Hence

$$\begin{cases} q(t) &= \rho_0(\sin(\Omega_1 t) + \sin(\Omega_2 t)), \\ z(t) &= \rho_0(\cos(\Omega_2 t) - \cos(\Omega_1 t)), \\ \dot{q}(t) &= \rho_0(\Omega_1 \cos(\Omega_1 t) + \Omega_2 \cos(\Omega_2 t)), \\ \dot{z}(t) &= \rho_0(\Omega_1 \sin(\Omega_1 t) - \Omega_2 \sin(\Omega_2 t)). \end{cases} \quad (10)$$

We focus now on the projection on the (q, \dot{q}) phase space. Similar results can be obtained for the projection on the (z, \dot{z}) phase space, due to structure of system (1).

Proposition 3 (Convex envelope on (q, \dot{q})). *Let (q, \dot{q}) evolve under (1) with the impulse disturbance (8), then the boundary set is given by*

$$x_\partial(\phi) = \rho_0 \left(\frac{(\cos \phi, \Omega_1^2 \sin \phi)}{\sqrt{\cos^2 \phi + \Omega_1^2 \sin^2 \phi}} + \frac{(\cos \phi, \Omega_2^2 \sin \phi)}{\sqrt{\cos^2 \phi + \Omega_2^2 \sin^2 \phi}} \right), \quad \phi \in [0, 2\pi]. \quad (11)$$

Proof. Let $\theta_i = \Omega_i t$, and define the ellipse boundary and filled ellipse respectively

$$C_\omega := \{(\sin \theta, \omega \cos \theta) : \theta \in [0, 2\pi]\}, \quad (12)$$

$$E_\omega := \{(x, y) : x^2 + (y/\omega)^2 \leq 1\}. \quad (13)$$

From (10), write

$$(q, \dot{q})(t) = \rho_0 (\sin \theta_1, \Omega_1 \cos \theta_1) + \rho_0 (\sin \theta_2, \Omega_2 \cos \theta_2), \quad (14)$$

which yields the exact projected set

$$\mathcal{S} = \rho_0 (C_{\Omega_1} + C_{\Omega_2}) \quad (15)$$

Now, we use the properties from Minkowski additions \oplus for convex hulls and support functions [20]. Taking the convex hull $\text{co}(\cdot)$ of \mathcal{S} , using $\text{co}(A + B) = \text{co}(A) \oplus \text{co}(B)$, and $\text{co}(C_\omega) = E_\omega$ gives

$$\text{co}(\mathcal{S}) = \rho_0 (E_{\Omega_1} \oplus E_{\Omega_2}). \quad (16)$$

For an axis-aligned ellipse E_ω , its support function is given by $h_{E_\omega}(u(\phi)) = \sqrt{\cos^2 \phi + \omega^2 \sin^2 \phi}$ for $u(\phi) = (\cos \phi, \sin \phi)$. Additivity of support functions under Minkowski sum gives

$$h_{\text{co}(\mathcal{S})}(u(\phi)) = \rho_0 (h_{E_{\Omega_1}}(u(\phi)) + h_{E_{\Omega_2}}(u(\phi))). \quad (17)$$

The boundary set (11) follows from the fact that strictly convex smooth sets have a unique exposed point in each direction, obtained by normalising the gradient of the support function. \square

Remark 1 (Ellipticity). The curve (11) is an ellipse iff $\Omega_1 = \Omega_2 = 1$, i.e. $n = 0$. Moreover, for $n \neq 0$ the boundary is the Minkowski addition of two unequal ellipses and is never itself an ellipse.

Remark 2 (Maximal radius). Energy conservation implies $q^2 + \dot{q}^2 \leq \dot{q}_0^2$ with equality at $t = 0$, consistent with $h_{\text{co}(\mathcal{S})}(u) = \dot{q}_0$ for $u = (0, 1)$.

A similar analysis can be done for (z, \dot{z}) . In Figure 1, the boundary set and the maximal radius is plotted for $n = 2$ and $n = 1/\sqrt{12}$, which is the resonant pair $(\tau, \sigma) = (4, 3)$ according to (7). Notice that in Figure 1a for $n = 2$, in absence of a resonant pair, the solution set is dense, and the envelope is clearly not elliptical. Figure 1b shows a closed Lissajous curve, thus the set is sparse.

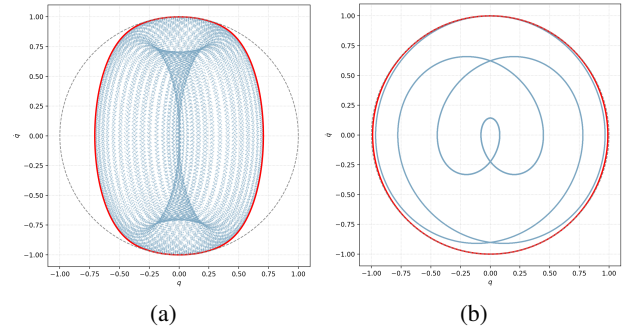


Fig. 1: The phase plane $(q(t), \dot{q}(t))$, $t \in [0, \frac{200\pi}{n}]$, of (1) for an impulse response $(\dot{q}_0 = 1)$ with (a) $n = 2$ and (b) $n = \frac{1}{\sqrt{12}}$. The boundary set x_∂ , given by (11) (full line, red), and maximal radius (dotted line) are plotted as well.

A. Resonant Lissajous curves

At a resonant pair (τ, σ) , define $\theta := \alpha t$, so q, \dot{q} depend on θ only through harmonics $\tau\theta$ and $\sigma\theta$. From $\Omega_1\Omega_2 = 1$ follows that $\Omega_1 = \Omega_2^{-1} = \sqrt{\frac{\tau}{\sigma}}$. So $(\tau\alpha, \sigma\alpha) = (\Omega_1, \Omega_2)$ iff $\alpha = \frac{1}{\sqrt{\tau\sigma}}$. Consider now the impulse response (10):

$$\begin{cases} q(\theta) = \rho_0 (\sin(\tau\theta) + \sin(\sigma\theta)), \\ \dot{q}(\theta) = \rho_0 (\sqrt{\frac{\tau}{\sigma}} \cos(\tau\theta) + \sqrt{\frac{\sigma}{\tau}} \cos(\sigma\theta)), \end{cases} \quad (18)$$

and the squared radius

$$R(\theta) = r(\theta)^2 = q(\theta)^2 + \dot{q}(\theta)^2. \quad (19)$$

B. Resonant inscribed circle

Define the resonant inscribed radius

$$r_{res} := \min_{\theta \in [0, 2\pi[} \sqrt{R(\theta)}. \quad (20)$$

The inscribed circle tells us the minimal amount of energy $H_{q,min} = \frac{1}{2}r_{res}^2$ that remains in the subsystem (q, \dot{q}) at all time. This is an interesting metric to evaluate or design a system if the coupling parameter n of (1) is tunable. The goal of this section is to understand the inscribed circle in the case of a resonant pair. Note that in non-resonant cases, the solution is dense in the phase space, as shown in Figure 1a, so it tends to have a very small inscribed circle.

Theorem 1 (Degenerate resonant inscribed circle). *Let (τ, σ) be a resonant pair and consider the resonant parametrisation (18). Then*

$$r_{res} = 0 \iff \delta := \tau - \sigma \equiv 2 \pmod{4}.$$

Moreover, in that case $R(\pi/2) = 0$, so the minimum is attained at $\theta^* = \pi/2 \pmod{\pi}$.

Proof. Using (18) and (19)

$$\frac{R(\theta)}{\rho_0^2} = (\sin(\tau\theta) + \sin(\sigma\theta))^2 + \left(\sqrt{\frac{\tau}{\sigma}} \cos(\tau\theta) + \sqrt{\frac{\sigma}{\tau}} \cos(\sigma\theta) \right)^2,$$

so $R(\theta) = 0$ iff

$$\begin{cases} \sin(\tau\theta) + \sin(\sigma\theta) = 0, \\ \sqrt{\frac{\tau}{\sigma}} \cos(\tau\theta) + \sqrt{\frac{\sigma}{\tau}} \cos(\sigma\theta) = 0. \end{cases} \quad (21)$$

Using the product-to-sum formula,

$$\sin(\tau\theta) + \sin(\sigma\theta) = 2 \sin\left(\frac{\tau+\sigma}{2}\theta\right) \cos\left(\frac{\tau-\sigma}{2}\theta\right),$$

the first equation in (21) holds if either (a) $\cos\left(\frac{\delta}{2}\theta\right) = 0$ or (b) $\sin\left(\frac{\tau+\sigma}{2}\theta\right) = 0$.

- *Case (a).* If $\cos\left(\frac{\delta}{2}\theta\right) = 0$, then $\tau\theta = \sigma\theta + \pi \pmod{2\pi}$, so $\cos(\tau\theta) = -\cos(\sigma\theta)$. Substituting into the second equation in (21) gives $\cos(\sigma\theta) (\sqrt{\frac{\sigma}{\tau}} - \sqrt{\frac{\tau}{\sigma}}) = 0$. Since $\tau \neq \sigma$, the coefficient is nonzero and therefore $\cos(\sigma\theta) = 0$. Hence $\theta = \frac{\pi}{2\sigma}(1+2k)$, $k \in \mathbb{Z}$. On the other hand, from $\cos\left(\frac{\delta}{2}\theta\right) = 0$ we obtain $\theta = \frac{\pi}{\delta}(1+2m)$, $m \in \mathbb{Z}$. Equating these two expressions for θ yields the Diophantine condition $\delta(1+2k) = 2\sigma(1+2m)$. Taking 2-adic valuations, the exponent of 2 in the prime factorisation, on both sides gives $v_2(\delta) = 1 + v_2(\sigma)$. Because $\gcd(\tau, \sigma) = 1$, at most one of τ or σ can be even. If σ were even, then τ is odd and δ would be odd, so $v_2(\sigma) = -1$, contradicting $\sigma \in \mathbb{N}$. Hence σ must be odd, so $v_2(\sigma) = 0$ and therefore $v_2(\delta) = 1$. Thus $\delta = 2(1+2r)$, $r \in \mathbb{Z}$, i.e. $\delta \equiv 2 \pmod{4}$.
- *Case (b).* If $\sin\left(\frac{\tau+\sigma}{2}\theta\right) = 0$, then $\frac{\tau+\sigma}{2}\theta = \pi k$, $k \in \mathbb{Z}$, and therefore $\cos(\tau\theta) = \cos(\sigma\theta)$. Substituting this into the second equation of (21) yields $\cos^2(\sigma\theta)(\tau - \sigma) = 0$. Since $\tau \neq \sigma$, the coefficient is nonzero, hence $\cos(\sigma\theta) = 0$. Thus $\theta = \frac{\pi}{2\sigma}(1+2m)$, $m \in \mathbb{Z}$. Together with $\frac{\tau+\sigma}{2}\theta = \pi k$, this gives $(\tau + \sigma)(1+2m) = 4\sigma k$. Taking 2-adic valuations on both sides and using $v_2(1+2m) = 0$ gives $v_2(\tau + \sigma) = 2 + v_2(\sigma) + v_2(k)$.

Since $\gcd(\tau, \sigma) = 1$, at most one of them is even. If σ were even, then τ would be odd and $\tau + \sigma$ odd, so $v_2(\tau + \sigma) = 0$, contradicting the above equality. Hence σ is odd, so $v_2(\sigma) = 0$ and therefore $v_2(\tau + \sigma) \geq 2$. In particular, both τ and σ are odd. Using

$$\begin{cases} 2\tau = (\tau + \sigma) + (\tau - \sigma), \\ 2\sigma = (\tau + \sigma) - (\tau - \sigma), \end{cases}$$

and the fact that $v_2(x+y) = \min(v_2(x), v_2(y))$ when $v_2(x) \neq v_2(y)$, we obtain from $v_2(2\tau) = v_2(2\sigma) = 1$ and $v_2(\tau + \sigma) \geq 2$ that $v_2(\tau - \sigma) = 1$. Hence $\delta \equiv 2 \pmod{4}$.

Hence, both branches lead to the same criterion.

Finally, if $\delta \equiv 2 \pmod{4}$ then τ, σ are odd with opposite residues mod 4, and at $\theta = \pi/2$ one has $\cos(\tau\pi/2) = \cos(\sigma\pi/2) = 0$ while $\sin(\tau\pi/2) = -\sin(\sigma\pi/2)$, giving $R(\pi/2) = 0$. \square

The classification of resonant pairs (τ, σ) for which the inscribed radius r_{res} vanishes plays a central conceptual role in our analysis. Indeed, the condition $\delta \equiv 2 \pmod{4}$ characterises precisely those commensurate frequency ratios for which the two modal ellipses become exact negatives of each other at a common phase, thereby producing complete cancellation of both displacement and velocity. This phenomenon is highly non-generic: it does not depend on the amplitude ρ_0 nor on the individual modal frequencies, but solely on an arithmetic property of the resonance pair. For the control

interpretation, these resonances mark precisely the regimes where passive gyroscopic coupling permits maximal energy exchange between modes. Consequently, the congruence condition $\delta \equiv 2 \pmod{4}$ is not merely a number-theoretic curiosity but a structurally meaningful criterion governing the attainable performance limits of the system.

Now, consider the case where $\delta \neq 2 \pmod{4}$.

Theorem 2. Consider the parametric Lissajous curve (18) with squared radius (19), and assume $\delta \not\equiv 2 \pmod{4}$. Let $\{\theta_i\}$ be the ordered roots of $q(\theta) = 0$ and $I_i = [\theta_i, \theta_{i+1}]$ the corresponding lobes of the Lissajous curve. Let $\theta_{c,i} \in]\theta_i, \theta_{i+1}[$ be the unique root of $\dot{q} = 0$ in lobe I_i . Let

$$\alpha(\theta) = \frac{\tau + \sigma}{2}\theta, \quad \beta(\theta) = \frac{\tau - \sigma}{2}\theta.$$

A lobe I_i will be called envelope-minimising if

$$\min_{\theta \in I_i} |\cos \beta(\theta)|$$

is globally minimal among all lobes. Then:

- 1) The global minimum of $r(\theta)$ is attained in an envelope-minimising lobe.
- 2) In any envelope-minimising lobe I_i , the function $R(\theta)$ is strictly decreasing on $[\theta_i, \theta_{c,i}]$ and strictly increasing on $[\theta_{c,i}, \theta_{i+1}]$. Consequently, $R(\theta)$ admits a unique minimiser in I_i , namely $\theta_{c,i}$.
- 3) Therefore

$$\min_{\theta \in [0, 2\pi]} r(\theta) = \min_i r(\theta_{c,i}) = \min_i |q(\theta_{c,i})|.$$

Proof. Introduce the constants

$$A = \frac{\tau + \sigma}{\sqrt{\tau\sigma}} > 0, \quad B = \frac{\sigma - \tau}{\sqrt{\tau\sigma}} < 0,$$

such that (18) can be rewritten to yield the expressions

$$\begin{cases} q(\theta) = 2\rho_0 \sin \alpha(\theta) \cos \beta(\theta), \\ \dot{q}(\theta) = \rho_0 (A \cos \alpha(\theta) \cos \beta(\theta) + B \sin \alpha(\theta) \sin \beta(\theta)). \end{cases} \quad (22)$$

Hence

$$R(\theta) = \rho_0^2 \begin{bmatrix} \sin \alpha \\ \cos \alpha \end{bmatrix}^\top M(\beta) \begin{bmatrix} \sin \alpha \\ \cos \alpha \end{bmatrix},$$

with the symmetric matrix

$$M(\beta) = \begin{pmatrix} 4 \cos^2 \beta + B^2 \sin^2 \beta & AB \sin \beta \cos \beta \\ AB \sin \beta \cos \beta & A^2 \cos^2 \beta \end{pmatrix}.$$

The eigenvalues of $M(\beta)$ satisfy

$$\begin{cases} \text{trace } M(\beta) = (A^2 + 4) \cos^2 \beta + B^2 \sin^2 \beta, \\ \det M(\beta) = 4A^2 \cos^4 \beta. \end{cases} \quad (23)$$

Let $\lambda_{\min}(\beta)$ denote the smallest eigenvalue. By the Rayleigh-Ritz principle,

$$R(\theta) \geq \rho_0^2 \lambda_{\min}(\beta(\theta)). \quad (24)$$

1) *Identification of envelope-minimising lobes:* Fix $\phi \in]0, 1]$. If a lobe I_j satisfies $|\cos \beta(\theta)| \geq \phi$ for all $\theta \in I_j$, then

$$\begin{aligned} \lambda_{\min}(\beta) &\geq \frac{\det M(\beta)}{\text{trace } M(\beta)} = \frac{4A^2 \cos^4 \beta}{(A^2 + 4) \cos^2 \beta + B^2 \sin^2 \beta} \\ &\geq c(\phi) = \frac{4A^2 \phi^4}{(A^2 + 4)\phi^2 + B^2(1 - \phi^2)} \\ &> 0. \end{aligned} \quad (25)$$

By (24), such a lobe satisfies

$$R(\theta) \geq \rho_0^2 c(\phi) \quad (\theta \in I_j).$$

Hence a global minimum cannot occur in lobes where $|\cos \beta|$ is bounded away from 0. The only candidates are lobes I_i that contain points where $|\cos \beta|$ becomes arbitrarily small. These are exactly the envelope-minimising lobes. Note there can exist multiple envelope-minimising lobes, but they will all lead to the same global minimum value.

2) *Monotonicity of R inside an envelope-minimising lobe:* Fix such a lobe $I_i = [\theta_i, \theta_{i+1}]$. Since the roots of q and \dot{q} interlace (trivial), there exists a unique interior point $\theta_{c,i} \in (\theta_i, \theta_{i+1})$ such that $\dot{q}(\theta_{c,i}) = 0$. Inside the envelope-minimising lobe, $|\cos \beta|$ is small whereas $|\sin \beta| \approx 1 - O(\cos^2(\beta))$. Consequently,

$$q(\theta) = O(\cos \beta), \quad q'(\theta) = O(\sin \beta),$$

and thus $qq' = O(\cos^2 \beta)$ is uniformly small across I_i , with $x'(\theta) = \frac{dx(\theta)}{d\theta}$. In contrast, the dominant components of \dot{q} and \dot{q}' are

$$\dot{q}(\theta) \approx \rho_0 B \sin \alpha(\theta), \quad \dot{q}'(\theta) \approx \rho_0 [B \alpha' - A \beta'] \cos \alpha(\theta).$$

Thus, up to a lobe-uniform nonzero factor, the sign of $\dot{q}(\theta)\dot{q}'(\theta)$ equals the sign of $\sin \alpha(\theta) \cos \alpha(\theta)$.

Since $\alpha(\theta)$ is strictly increasing and $\dot{q}(\theta_{c,i}) = 0$ implies $\sin \alpha(\theta_{c,i}) = 0$ with $\cos \alpha(\theta_{c,i}) \neq 0$, we have:

$$\begin{cases} \dot{q}\dot{q}' < 0 & \forall \theta \in]\theta_i, \theta_{c,i}[, \\ \dot{q}\dot{q}' > 0 & \forall \theta \in]\theta_{c,i}, \theta_{i+1}[. \end{cases} \quad (26)$$

Note that the zero of \dot{q} is simple: $\dot{q}'(\theta_{c,i}) \neq 0$, since otherwise \dot{q} and \dot{q}' would vanish simultaneously, forcing $\delta\theta \in \pi\mathbb{Z}$ and $\cos \beta = 0$, compatible only when $\delta \equiv 2 \pmod{4}$, which is excluded.

Now compute

$$R'(\theta) = 2(qq' + \dot{q}\dot{q}').$$

Because $qq' = O(\cos^2 \beta)$ is uniformly small in I_i , while $\dot{q}\dot{q}'$ has strict sign on each side of $\theta_{c,i}$, it follows that

$$R'(\theta) < 0 \text{ on }]\theta_i, \theta_{c,i}[, \quad R'(\theta) > 0 \text{ on }]\theta_{c,i}, \theta_{i+1}[.$$

Therefore R is strictly decreasing on $]\theta_i, \theta_{c,i}[$ and strictly increasing on $]\theta_{c,i}, \theta_{i+1}[$. Hence $\theta_{c,i}$ is the *unique* minimiser of R on I_i . Any endpoint θ_i or θ_{i+1} at which $R'(\theta)$ may vanish is necessarily a local maximum, since the sign pattern of R' is strictly negative immediately to the right of θ_i and strictly positive immediately to the left of θ_{i+1} .

3) *Global minimality:* As shown in Part 1, the global minimiser must lie in an envelope-minimising lobe. Part 2 shows that within any such lobe the unique minimizer is $\theta_{c,i}$, proving the theorem. \square

So from Theorem 2, the minimal energy occurs near the slow-mode zero

$$\beta = \frac{\delta}{2}\theta = \frac{\pi}{2} \Rightarrow \theta \approx \frac{\pi}{\delta},$$

or, equivalently, near $T_{\min} \approx \pi/n$. Furthermore, it is shown in Theorem 2 that the minimum is attained at the unique root of $\dot{q}(\theta) = 0$ inside the interval close to $\theta_0 = \pi/\delta$ at which $|q(\theta)|$ is minimal (see Figure 1b). However, a closed form for this root is unavailable, so we introduce a systematic asymptotic approximation based on the slow-mode reduction.

Set

$$a := \tau + \sigma, \quad b := \tau - \sigma, \quad x := \frac{b}{a} \in]0, 1[,$$

and so $\alpha = \frac{a}{2}\theta$, $\beta = \frac{b}{2}\theta = x\alpha$. Next, we propose a coordinate shift, such that the fast phase is a deviation u from the k^{th} node: $\alpha = k\pi + u$ with $u \in]-\pi/2, \pi/2[$ and $k = \text{round}(1/(2x))$. We introduce $\mu = \frac{\pi}{2} - k\pi x$ and $s = \frac{\mu}{x}$, which is the phase lag between the fast-mode node and slow-mode node. Now, we propose a reduced extremum condition for $\dot{q}(\theta) = 0$ which will lead to an asymptotic proxy for the true minimising phase.

Theorem 3. *Let θ_c denote the unique solution of $\dot{q}(\theta) = 0$ near the slow-mode node $\theta_0 = \pi/b$. Then the first-order asymptotic approximation of θ_c is*

$$\theta_{\text{asy}} = \frac{\pi}{b} + \frac{2}{a} (u_{\text{asy}} - s), \quad (27)$$

where u_{asy} is the unique solution of

$$u + \tan u = s. \quad (28)$$

Proof. Substituting $\alpha = k\pi + u$ into $\beta = x\alpha$ and using the identities

$$\tan \alpha = \tan u, \quad \tan^{-1} \beta = \tan(\mu - xu),$$

the condition $\dot{q}(\theta) = 0$ reduces exactly to $x \tan u = \tan(\mu - xu)$. Expanding $\tan(\mu - xu)$ in x , yields $\tan(\mu - xu) = \tan \mu - xu \sec^2 \mu + O(x^2)$. Neglecting the higher-order term, and notice that μ is small for k as defined above ($\tan(\mu) \approx \mu$ and $\sec^2(\mu) \approx 1$), such that the first-order approximation $x \tan u \approx \tan \mu - xu \sec^2 \mu$ simplifies to $u + \tan u = s$. Reconstructing θ from $\alpha = \frac{a}{2}\theta = k\pi + u$ yields the stated expression. \square

The next theorem provides a closed, uniform bound on the approximation error and quantifies the accuracy of θ_{asy} .

Theorem 4. *With θ_{asy} as in Theorem 3, the approximation error obeys*

$$|\theta_c - \theta_{\text{asy}}| \leq \frac{\pi^3}{a} x^2 = \pi^3 \frac{(\tau - \sigma)^2}{(\tau + \sigma)^3}. \quad (29)$$

Hence the approximation is $O((\tau - \sigma)^2/(\tau + \sigma)^3)$ uniformly over all coprime (τ, σ) .

Proof. Let $g(u) = x(\tan u + u)$. The exact condition $\dot{q}(\theta_c) = 0$ is $x \tan u_c = \tan(\mu - xu_c)$. Expanding the right-hand side via Taylor's theorem yields $x \tan u_c = (\mu - xu_c) + \Delta u$, which simplifies to $g(u_c) = \mu + \Delta u$. Our approximation u_{asy} satisfies $g(u_{\text{asy}}) = \mu$ by construction. By the Mean Value Theorem:

$$|u_c - u_{\text{asy}}| = \frac{|g(u_c) - g(u_{\text{asy}})|}{|g'(\xi)|} = \frac{|\Delta u|}{x(1 + \sec^2 \xi)} \leq \frac{|\Delta u|}{2x}, \quad (30)$$

where $\xi \in]u_c, u_{\text{asy}}[$ and $1 + \sec^2 \xi \geq 2$. Next, we bound the remainder Δu using the Lagrange form $R_1 = \frac{1}{2}f''(\zeta)(xu)^2$ for $f(z) = \tan z$. With $|u| \leq \pi/2$ and the evaluation point $|\zeta| \leq |\mu| + x|u| \leq \pi x$, we have:

$$|\Delta u| = |x^2 u^2 \sec^2 \zeta \tan \zeta| \leq \pi^3 x^3, \quad (31)$$

where we used $\tan(\pi x) \leq 2\pi x$ and $\sec^2(\pi x) \leq 2$ for small x . Combining these results yields $|u_c - u_{\text{asy}}| \leq \frac{\pi^3 x^2}{2}$. Since $\theta = \frac{2}{a}(k\pi + u)$, the parameter error bound (29) is found. For $x \ll 1$, this $O(a^{-3})$ bound confirms the high precision of the asymptotic proxy. \square

The asymptotic reduction from $\dot{q}(\theta) = 0$ to the scalar equation $u + \tan(u) = s$ does not eliminate numerical computation; it merely transfers the root-finding task from the phase variable θ_c to the reduced variable u . Consequently, the computational gain is not fundamental. The principal value of the reduction is structural: the equation $u + \tan(u) = s$ is independent of the small parameter $x = (\tau - \sigma)/(\tau + \sigma)$, it isolates the slow-mode geometry through the fixed interval $u \in [-\pi/2, \pi/2]$ and the unique solution on that interval, and it enables a closed-form reconstruction θ_{asy} (27) together with a uniform error bound (29). These features provide analytic insight and parameter-uniform guarantees that are difficult to obtain via direct numerical solution of $\dot{q}(\theta) = 0$. However, in settings where such analytical guarantees are not required, a well-bracketed numerical method applied directly to $\dot{q}(\theta) = 0$ can deliver the exact root to machine precision with comparable effort, especially when x is not small or when the slow-mode localisation offers limited advantage.

IV. CONTROLLER DESIGN

From a control theoretical point of view, we can discern (q, \dot{q}) as a host subsystem and (z, \dot{z}) as an auxiliary/controller, connected through a power-preserving port with storage function H [18]. The inscribed radius bound r_{res} furnishes an *internal performance certificate* consistent with passivity and dissipativity theory [5], [9], [10], [21].

As mentioned in Section III, consider the closed-loop class induced by shaping the constant gyroscopic interconnection strength $n \in \mathbb{R}$ (and, optionally, kinetic/potential scalings that preserve the quadratic Hamiltonian form), subject to the impulse disturbance class \mathcal{D} in (8). With the above, we can obtain for each choice of n and each disturbance in \mathcal{D} the largest origin-centered circle with radius $r_{\text{res}}(n; \dot{q}_0)$ inscribed

in the *projected* subsystem trajectory on (q, \dot{q}) (or equivalently on (z, \dot{z}) by symmetry). By linearity,

$$r_{\text{res}}(n; \dot{q}_0) = |\dot{q}_0| r_{\text{res}}(n; 1). \quad (32)$$

Equivalently,

$$\min_{t \geq 0} H_q(t) = \frac{1}{2} r_{\text{res}}(n; \dot{q}_0)^2.$$

Both the largest inscribed circle radius r_{res} and the estimated time to reach said minimum T_{\min} (for the first time) can be used to obtain an optimal controller design. Recall that $T_{\min} \approx \frac{\pi}{|n|}$, and in a resonant case $T_{\min} = \sqrt{\tau\sigma}\theta_c$. Two design problems can be discerned:

- **Absorption with speed constraint:**

$$\min_{n \in \mathcal{N}} r_{\text{res}}(n; D) \quad \text{s.t.} \quad T_{\min}(n) \leq T_{\max}, \quad (33)$$

and the optional exclusion $\Omega_1 : \Omega_2 \notin \mathcal{R}_{\text{low}}$ avoids low-order locking sets that inflate r_{res} .

- **Containment with responsiveness:**

$$\max_{n \in \mathcal{N}} r_{\text{res}}(n; D) \quad \text{s.t.} \quad T_{\min}(n) \leq T_{\max}. \quad (34)$$

Remark 3 (Pareto frontier). The set $\{(r_{\text{res}}(n; 1), T_{\min}(n))\}_{n \in \mathcal{N}}$ defines a Pareto frontier. Low-order locking points (large n) give fast but conservative exchange (large r_{res}), whereas near-irrational points (small n) give deep exchange (small r_{res}) but slow attraction. This is clearly demonstrated in Figure 2, where r_{res} is plotted in function $\log(1 + T_{\min})$ for different resonant pairs (τ, σ) . The red line shows a clear trade-off between both performance metrics.

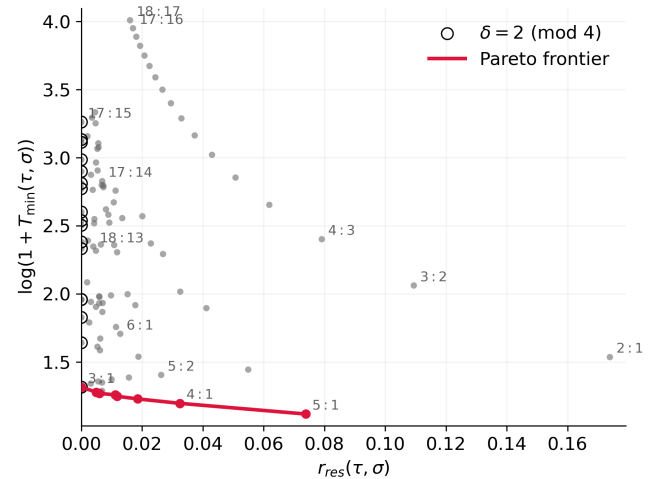


Fig. 2: The Pareto frontier of speed vs. minimum energy. Schematic plot of $(r_{\text{res}}(n(\tau, \sigma); 1), T_{\min}(n(\tau, \sigma)))$ as (τ, σ) varies. Note the low-order resonances (fast/large) and near-irrational ratios (slow/small).

V. EXAMPLES

We consider the gyroscopically coupled, conservative 2-DOF system (1) with an impulse disturbance (8) with $\dot{q}_0 = 1$. We present two examples where n needs to be designed. Following prior absorber design practice, we require a pronounced beat:

$$\frac{\tau + \sigma}{\tau - \sigma} \geq 10, \quad (35)$$

so that one slow envelope period contains at least ten fast cycles.

A. Case A - Absorption

We target $\delta \equiv 2 \pmod{4}$ to enable complete cancellation (zero inscribed radius) and preferably as fast as possible, as in (33). With $\delta = 2$, (35) gives $\tau \geq 11$ and, thus, $\sigma \geq 9$, and the pair $(11, 9)$ is coprime. This gives $n = 0.201$ and $T_{\min} \approx 15.6s$. With $\delta = 6$, (35) gives $\tau \geq 33$, so the smallest coprime that agrees to these conditions is $(41, 35)$, but $T_{\min} \approx 19.8s$, so this is worst and will only deteriorate if we increase δ further (see Figure 2). So for $(\tau, \sigma) = (11, 9)$, the Lissajous trajectory in (q, \dot{q}) is closed and intersects the origin, so $r_{\min} = 0$. Furthermore is the beat pronounced and is the time to achieve zero energy minimal. Figure 3 shows the phase portrait with the closed, sparse Lissajous curve, the analytic convex boundary (Minkowski-sum envelope), and the largest origin-centered inscribed circle (degenerate). Figure 4 shows $H_q(t)$ with the predicted T_{\min} marker.

B. Case B - Containment

Here, we want to achieve design criterium (34). We require resonance for a sparse (non-dense) trajectory but avoid $\delta \equiv 2 \pmod{4}$. From Figure 2 it is clear that $\delta = 1$ leads to large r_{res} . Then from (35) it follows that $\tau \geq 5.5$. As $\tau \in \mathbb{N}$ the coprime pair $(\tau, \sigma) = (6, 5)$ is chosen. Then $n = 0.183$, and $T_{\min} \approx 17.2s$. Here, the Lissajous trajectory is closed and remains away from the origin. To find the resonant inscribed radius, we find from (28) that $u_{\text{asy}} = -0.17\text{rad}$, which gives $\theta_{\text{asy}} = 3.30\text{rad}$. This is validated as $\dot{q}(\theta_{\text{asy}}) = 2.43 \times 10^{-4}$, and (29) leads to $|\theta_c - \theta_{\text{asy}}| = 1.16 \times 10^{-4} \leq 2.33 \times 10^{-2}$. This yields $r_{\min} = 5.075 \times 10^{-2}$, i.e., a certified lower bound on H_q . Figure 5 shows the phase portrait with the trajectory, envelope, and the nonzero inscribed circle. Figure 6 shows $H_q(t)$ and the T_{\min} marker.

VI. CONCLUSIONS

We presented a geometric and computational analysis of energy exchange in gyroscopic systems, deriving exact envelopes, explicit resonance conditions, and introducing the resonant inscribed radius as a metric to quantify the minimal energy that remains confined to a subsystem for any resonant pair (τ, σ) , which determines a unique coupling parameter n . Degeneracy of this metric occurs precisely when $\tau - \sigma \equiv 2 \pmod{4}$. In all other cases, we provided a numerical procedure to compute the resonant inscribed radius together with a uniform error bound. Finally, we connected these insights to a controller design framework for targeted

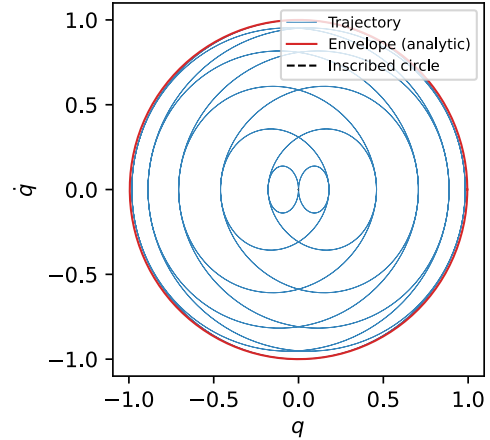


Fig. 3: Absorption case (11,9): phase portrait with envelope and inscribed circle.

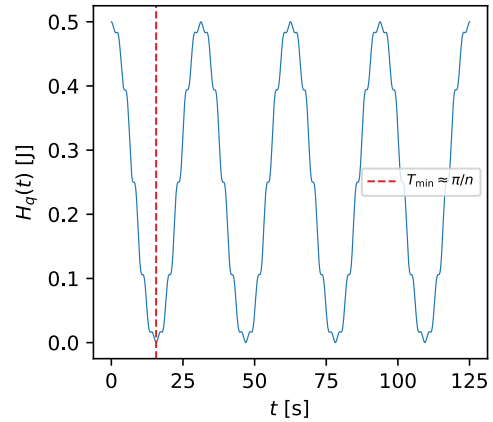


Fig. 4: Absorption case (11,9): subsystem energy $H_q(t)$ with $T_{\min} \approx \pi/n$ marker.

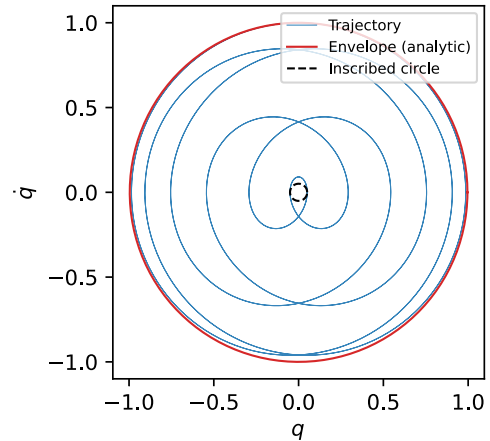


Fig. 5: Containment case (6,5): phase portrait with envelope and inscribed circle.

energy absorption and containment within a subsystem, and illustrated the methodology through representative examples.

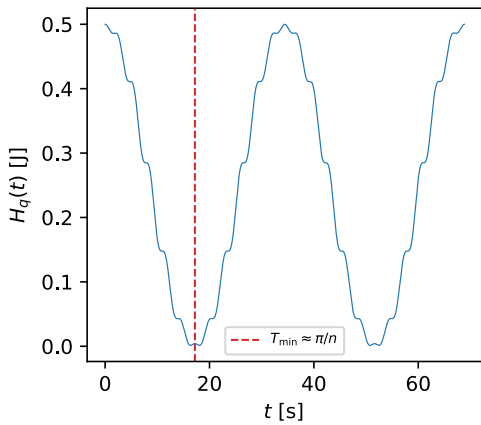


Fig. 6: Containment case (6,5): subsystem energy $H_q(t)$ with $T_{\min} \approx \pi/n$ marker.

- [16] M. Morlans, J. Guérard, and J. Juillard, “Characterization of electrical and mechanical coupling in mems gyroscopes with electrical measurements,” in *2021 Symposium on Design, Test, Integration & Packaging of MEMS and MOEMS (DTIP)*, Paris, France, 2021.
- [17] R. Ortega, A. van der Schaft, F. Castanos, and A. Astolfi, “Control by interconnection and standard passivity-based control of port-hamiltonian systems,” *IEEE Transactions on Automatic Control*, vol. 53, no. 11, pp. 2527–2542, 2008.
- [18] J. Juchem, S. Geyskens, K. Dekemele, and M. Loccuif, “A virtual mechanical system control law for energy transfer towards a single actuation point in n dof buildings,” *Engineering Structures*, vol. 302, p. 117493, 2024.
- [19] V. I. Arnold, *Mathematical Methods of Classical Mechanics*, 2nd ed. Springer, 1989.
- [20] R. Schneider, *Convex Bodies: The Brunn–Minkowski Theory*. Cambridge University Press, 2014.
- [21] W. M. Haddad and V. Chellaboina, *Nonlinear Dynamical Systems and Control: A Lyapunov-Based Approach*. Princeton University Press, 2008.

REFERENCES

- [1] A. M. Bloch, N. E. Leonard, and J. E. Marsden, “Controlled lagrangians and the stabilization of mechanical systems. i. the first matching theorem,” *IEEE Transactions on Automatic Control*, vol. 45, no. 12, pp. 2253–2270, 2000.
- [2] A. M. Bloch, D. E. Chang, N. E. Leonard, and J. E. Marsden, “Controlled lagrangians and the stabilization of mechanical systems ii: Potential shaping,” *IEEE Transactions on Automatic Control*, vol. 46, no. 10, pp. 1556–1571, 2001.
- [3] R. Ortega, A. J. van der Schaft, B. Maschke, and G. Escobar, “Interconnection and damping assignment passivity-based control of port-controlled hamiltonian systems,” *Automatica*, vol. 38, no. 4, pp. 585–596, 2002.
- [4] B. M. Maschke and A. J. van der Schaft, “Port-controlled hamiltonian systems: Modelling origins and systemtheoretic properties,” in *Proc. IFAC Symp. Nonlinear Control Systems Design*, 1992, pp. 282–288.
- [5] A. van der Schaft, *L_2 -Gain and Passivity Techniques in Nonlinear Control*, 2nd ed. Springer, 2000.
- [6] C. A. Woolsey, C. K. Reddy, A. M. Bloch, D. E. Chang, N. E. Leonard, and J. E. Marsden, “Controlled lagrangian systems with gyroscopic forcing and dissipation,” *European Journal of Control*, vol. 10, no. 5, pp. 1–27, 2004.
- [7] G. Blankenstein, R. Ortega, and A. J. van der Schaft, “The matching conditions of controlled lagrangians and ida-passivity based control,” *International Journal of Control*, vol. 75, no. 9, pp. 645–665, 2002.
- [8] V. Duindam, A. Macchelli, S. Stramigioli, and H. Bruyninckx, *Modeling and Control of Complex Physical Systems*. Springer Berlin, Heidelberg, 2009.
- [9] J. C. Willems, “Dissipative dynamical systems,” *European Journal of Control*, vol. 13, no. 2–3, pp. 134–151, 2007.
- [10] D. J. Hill and P. J. Moylan, “The stability of nonlinear dissipative systems,” *IEEE Transactions on Automatic Control*, vol. 21, no. 5, pp. 708–711, 1976.
- [11] A. Katok and B. Hasselblatt, *Introduction to the Modern Theory of Dynamical Systems*. Cambridge University Press, 1995.
- [12] A. Pikovsky, M. Rosenblum, and J. Kurths, *Synchronization: A Universal Concept in Nonlinear Sciences*. Cambridge University Press, 2001.
- [13] X. Zhou, C. Zhao, D. Xiao, J. Sun, G. Sobreviela, D. D. Gerrard, Y. Chen, I. Flader, T. W. Kenny, X. Wu, and A. A. Seshia, “Dynamic modulation of modal coupling in microelectromechanical gyroscopic ring resonators,” *Nature Communications*, vol. 10, p. 4980, 2019.
- [14] F. Pistorio, M. M. Saleem, and A. Somà, “A dual-mass resonant MEMS gyroscope design with electrostatic tuning for frequency mismatch compensation,” *Applied Sciences*, vol. 11, no. 3, p. 1129, 2021.
- [15] Y. S. Hamed, A. T. El-Sayed, and E. R. El-Zahar, “On controlling the vibrations and energy transfer in MEMS gyroscope system with simultaneous resonance,” *Nonlinear Dynamics*, vol. 83, pp. 1687–1704, 2016.